

Reaction Pathway and Rovibrational Analysis of Aluminum Nitride Species as Potential Dust Grain Nucleation Agents

C. ZACHARY PALMER ¹ AND RYAN C. FORTENBERRY ¹

¹*Department of Chemistry & Biochemistry, University of Mississippi,
University, Mississippi, 38677, United States*

(Dated: January 15, 2024)

ABSTRACT

A dust nucleating agent may be present in interstellar or circumstellar media that has gone seemingly undetected and unstudied for decades. Some analyses of the Murchison CM2 meteorite suggest that at least some of the aluminum present within condensed as aluminum nitrides instead of the long studied, but heretofore undetected suite of aluminum oxides. The present theoretical study utilizes explicitly correlated coupled cluster theory and density functional theory to provide a pathway of formation from alane (AlH₃) and ammonia to the cyclic structure, Al₂N₂H₄ which has the proper Al/N ratio expected of bulk aluminum nitrides. Novel rovibrational spectroscopic constants are computed for alane and the first two formed structures, AlNH₆ and AlNH₄, along the reaction pathway for use as reference in possible laboratory or observational studies. The ν_8 bending frequency for AlNH₆ at 755.7 cm⁻¹ (13.23 μ m) presents a vibrational transition intensity of 515 km mol⁻¹, slightly more intense than the anti-symmetric C–O stretch of carbon dioxide, and contains a dipole moment of 5.40 D, which is $\sim 3\times$ larger than that of water. Thus, the present reaction pathway and rovibrational spectroscopic analysis may potentially assist in the astrophysical detection of novel, inorganic species which may be indicative of larger dust grain nucleation.

Keywords: Astrochemistry (75) — Interdisciplinary astronomy (804) — Neutral-neutral reactions (2265) — Quantum-chemical Calculations (2232) — Molecular spectroscopic constants (2260)

1. INTRODUCTION

Previous study (Zimmer et al. 1991) of the Murchison CM2 chondritic meteorite seems to suggest the aluminum present within condensed as a form of aluminum nitride rather than the more commonly assumed aluminum oxides. However, aluminum nitride clusters must compete with these aluminum oxides during dust grain nucleation and further formation. Alumina (Al₂O₃) is a common aluminum oxide that has been theorized as a major contributor to both bulk aluminum oxides and their use in dust grain nucleation and formation in the interstellar medium (ISM) and in circumstellar media (CSM) (Gail & Sedlmayr 1998, 1999; Gobrecht et al. 2016). One of the most commonly attributed spectral features for bulk alumina’s Al–O vibrational stretching and bending motions is seen at 13 μ m (Gobrecht et al. 2022; Sloan et al. 2003). Additionally, previous studies (Gail & Sedlmayr 1999; Sloan et al. 2003) attribute emission features at 11, 20, 28, and 32 μ m to the same carrier as the 13 μ m feature. Despite this, monomeric forms of aluminum oxides like Al₂O₃ have yet to be detected as their formation seems to be unfavorable due to many pathways hindered by endothermicities (Chang et al. 1998; Patzer et al. 2005; Gobrecht et al. 2022). Further, bulk-phase aluminum oxides exhibit high condensation temperatures that lead to reaction timescales that are too rapid to adequately detect such clusters (Lodders 2003). The presence of Al₂O₃ in chondritic meteorite studies suggests its existence in these stellar environments; without astronomical detection, though, their potential role in dust grain nucleation to formation cannot be confirmed (Nittler et al. 2008; Hutcheon et al. 1994). Thus, an investigation into an alternative Al-containing species that may not condense on timescales as quickly as Al₂O₃ is warranted to elucidate long-sought-after dust formation pathways containing Al that have eluded astrochemists and astrophysicists to date.

While Al condensates show high refractory character (Lodders 2003), not all of its forms, in CSM, condense into large bulk solids early in stellar evolution and evade detection. Within the circumstellar envelope of IRC+10216, amongst other oxygen-rich sources, two Al-halide species have been observed in the form of AlCl and AlF (Cernicharo & Guélin 1987; Ziurys et al. 1994; Decin et al. 2017; Saberi et al. 2022). These Al-halides have also been observed within circumstellar envelopes with C/O \sim 1 (Danilovich, T. et al. 2021). While these have been observed closer to the star, upon their ejection to the cooler regions of the stellar envelope, they are thought to deplete onto dust grains eluding any further detection. However, this is not the case for AlNC, which has been detected in larger concentrations within the cooler regions of the envelope and under the condensation temperature of the elusive Al₂O₃ molecule and other aluminum oxide clusters (Ziurys et al. 2002). The presence of the Al-halides and AlNC suggests that Al-containing species are not solely locked up into aluminum oxide clusters or grains. Thus, O-deficient, Al-containing species can be formed within the warmer regions of the stellar envelope and persist long enough in the cooler, outer circumstellar dust clouds before depositing or aggregating and disappearing from rovibrational detection.

Additionally, a radioisotope of Al, ²⁶Al, was identified in its fluorinated form, ²⁶AlF, near the stellar merger of CK Vulpus (Kamiński et al. 2018). ²⁶AlF is believed to have been introduced into the surrounding stellar region during the collision of the binary system yet persisted on a timescale long enough for detection (Kamiński 2015). Much like the elusive Al₂O₃, both the stable ²⁷Al and an extinct form of ²⁶Al, which later decayed into the ²⁶Mg isotope based on isotopic abundance studies, were found within the Murchison CM2 chondritic meteorite. An investigation of the ratio of ²⁶Al/²⁷Al suggests that the ²⁶Al present is in larger abundance in at least this meteorite compared to the ratio in the solar system at large. In any case, the presence of an aluminum nitride system within Murchison CM2 is suggested *via* a comparison of the SiC abundance and CN⁻/C⁻ ratio and the Al and N present within. Such a correlation suggests that the Al in the meteorite condensed not as some form of aluminum oxide, like Al₂O₃, but rather as some form of aluminum nitride system (Zinner et al. 1991). As discussed previously, the Al–N moiety is not unheard of in CSM from the presence of AlNC. Previous computational studies have calculated an Al–N bond strength of -105.0 kcal mol⁻¹, which is stronger than the bond strength of the N–C bond at -77.8 kcal mol⁻¹ (Doerksen & Fortenberry 2020). This larger bond strength of the Al–N bond, relative to the N–C bond in AlNC, suggests the stability of Al–N bonds in CSM and the ISM.

The study of the Murchison CM2 meteorite implies that the aluminum nitride systems present within play a key role in the nucleation of the graphite that composes the bulk of the carbonaceous material within the meteor by catalyzing the graphite’s inhibited nucleation (Czyzak et al. 1982; Nuth 1985; Zinner et al. 1991). With that, these new Al-containing species may be instrumental for the nucleation of aggregated material onto other solar system bodies, such as comets, asteroids, and other meteors. That being said, these conclusions justify an investigation into the presence of unreported aluminum nitride molecular systems in CSM and the ISM that may potentially assist in elucidating the processes of how Al-bearing species get from the gas phase into their bulk solid-phase dust grain counterparts.

As aluminum nitride systems have not been characterized in any stellar environment, no gas-phase observational or experimental spectroscopic data are available to begin the search for such species. Thus, the present quantum chemical study provides reference data for a proposed pathway of formation from the aluminum hydride, alane, (AlH₃) and ammonia (NH₃) into the first cyclic species along said pathway. Regardless of the AlH₃ molecule’s lack of interstellar detection, the present study utilizes AlH₃ as the main source of aluminum given its simplicity as a metal hydride and its closed-shell configuration. The AlH₃ molecule is used in place of the more simple, and previously detected (Kamiński, T. et al. 2016), aluminum mono-hydride (AlH) as previous computational studies suggest that access to more hydrogen atoms assists the progress of the reaction pathway (Grosselin & Fortenberry 2022; Flint & Fortenberry 2023). The rovibrational spectroscopic data herein will be instrumental in supporting the currently available spectroscopic telescopes and observational technologies like the *James Webb Space Telescope* (JWST) for its efficiency in probing the near- to mid-IR spectrum with its Near-Infrared Spectrograph (NIRSpec) and Mid-Infrared Instrument (MIRI) instruments. Where available, the provided rotational data will assist microwave spectroscopic observatories like the *Atacama Large Millimeter/sub-millimeter Array* (ALMA). To that end, the rovibrational spectroscopic analysis provided should aid in the potential astrophysical identification of aluminum nitride species that have yet to be characterized and may contribute to the dust grain nucleation and formation processes present in CSM and the ISM.

2. COMPUTATIONAL METHODS

2.1. Reaction Mechanism Methods

Unless otherwise stated, all geometry optimizations, single-point energy (SPE) computations, and zero-point vibrational energy corrections for the reactants, intermediates, and products of the aluminum nitride reaction pathway are conducted utilizing coupled cluster theory at the singles, doubles, and perturbative triples level [CCSD(T)] (Raghavachari et al. 1989; Shavitt & Bartlett 2009; Crawford & Schaefer III 2000). For an additional gain in accuracy, the CCSD(T) level of theory is corrected within the explicitly correlated F12b formalism (Adler et al. 2007; Knizia et al. 2009) along with its corresponding cc-pVTZ-F12 basis set (Peterson et al. 2008; Yousaf & Peterson 2008). The aforementioned level of theory will henceforth be abbreviated as “F12-TZ.” Geometry optimization and harmonic frequency computations for all transition states along the pathway are conducted with the B3LYP density functional (Yang et al. 1986; Lee et al. 1988) along with the aug-cc-pVTZ correlation consistent Dunning basis set (Kendall et al. 1992). After the transition states are optimized at the B3LYP/aug-cc-pVTZ level of theory, single-point energy computations are computed at the F12-TZ level (Ramal-Olmedo et al. 2021), and are subsequently corrected with B3LYP/aug-cc-pVTZ zero-point vibrational energies (ZPVEs). All minima along the reaction pathway are computed *via* the MOLPRO 2022.2 suite of quantum chemical packages (Werner et al. 2020). Finally, all transition state computations on the pathway are conducted *via* GAUSSIAN16 (Frisch et al. 2016).

2.2. Rovibrational Spectroscopic Methods

The highly accurate rovibrational spectroscopic constants are computed utilizing the quartic force field (QFF) approach. A QFF is a fourth-order Taylor series expansion of the potential energy portion of the internuclear Watson Hamiltonian (Fortenberry & Lee 2019). QFFs as employed herein have been able to produce rovibrational spectroscopic constants within 1% of experimental values for many molecular systems (Huang & Lee 2008, 2009; Huang et al. 2011; Zhao et al. 2014; Huang et al. 2013; Fortenberry et al. 2014, 2015; Kitchens & Fortenberry 2016; Fortenberry 2017; Fortenberry et al. 2018; Gardner et al. 2021). F12-TZ has been shown to produce accurate fundamental vibrational frequencies and rotational constants at far less computational cost compared to other QFF methods (Martin & Kesharwani 2014; Agbaglo et al. 2019; Agbaglo & Fortenberry 2019; Inostroza-Pino et al. 2020; Palmer & Fortenberry 2022). Additionally, the QFF implemented in this work is conducted within the recently developed automated PBQFF framework (Westbrook & Fortenberry 2023). The PBQFF procedure begins with a geometry optimization utilizing MOLPRO (Werner et al. 2020) at the F12-TZ level of theory with tight convergence criteria. From there, the optimized Cartesian geometry is displaced by 0.005 Å respective of bond lengths or angles, to mimic a QFF but is truncated to the second-order yielding a Cartesian harmonic force field. SPE computations for every displacement are computed and used to generate a harmonic force constant (FC) matrix. The normal coordinates are then extracted from the resulting mass-weighted Hessian matrix for the given molecular species. The optimized molecular geometry is then displaced along these normal coordinates to compute the rest of the semi-diagonal QFF, and SPE computations are performed at each normal coordinate displacement.

Once the SPE computations are finished, the final normal FCs are computed directly utilizing a finite differences procedure. The normal coordinate FCs are then passed to a second-order vibrational and rotational perturbation theory (VPT2) (Mills 1972; Watson 1977; Papoušek & Aliev 1982; Franke et al. 2021) algorithm within the PBQFF framework itself. From this, the harmonic frequencies, fundamental anharmonic vibrational frequencies, vibrationally-averaged rotational constants, singly-vibrationally-excited rotational constants, quartic distortion constants, and sextic distortion constants are produced. Additionally, if present in the analysis, the type-1 and -2 Fermi resonances and Coriolis resonances are taken into account as it has been shown to increase the accuracy of the computed rovibrational spectroscopic constants (Martin & Taylor 1997; Martin et al. 1995). To further assist in potential astrophysical detection, dipole moments for AlNH₆ and AlNH₄ are computed at the F12-TZ level within MOLPRO 2022.2 (Werner et al. 2020). Finally, double-harmonic infrared intensities computed using GAUSSIAN16 (Frisch et al. 2016) at the MP2/cc-pVDZ (Møller & Plesset 1934; Dunning 1989) level of theory are included to assist in the detection of these species in the infrared (IR). Computed intensities at this level of theory have been shown to produce semi-quantitative agreement with higher levels of theory for far less computational costs (Yu et al. 2015; Finney et al. 2016; Westbrook et al. 2021).

In addition to IR intensities, absorption cross sections, σ , are given for all applicable vibrational frequencies. The absorption cross sections are derived utilizing the formula in EQ. 1, where “ N_a ” is Avogadro’s number, and “ ϵ ” is the molar absorption coefficient.

$$\sigma = \frac{\ln(10) \times 10^3}{N_a} \times \epsilon \quad (1)$$

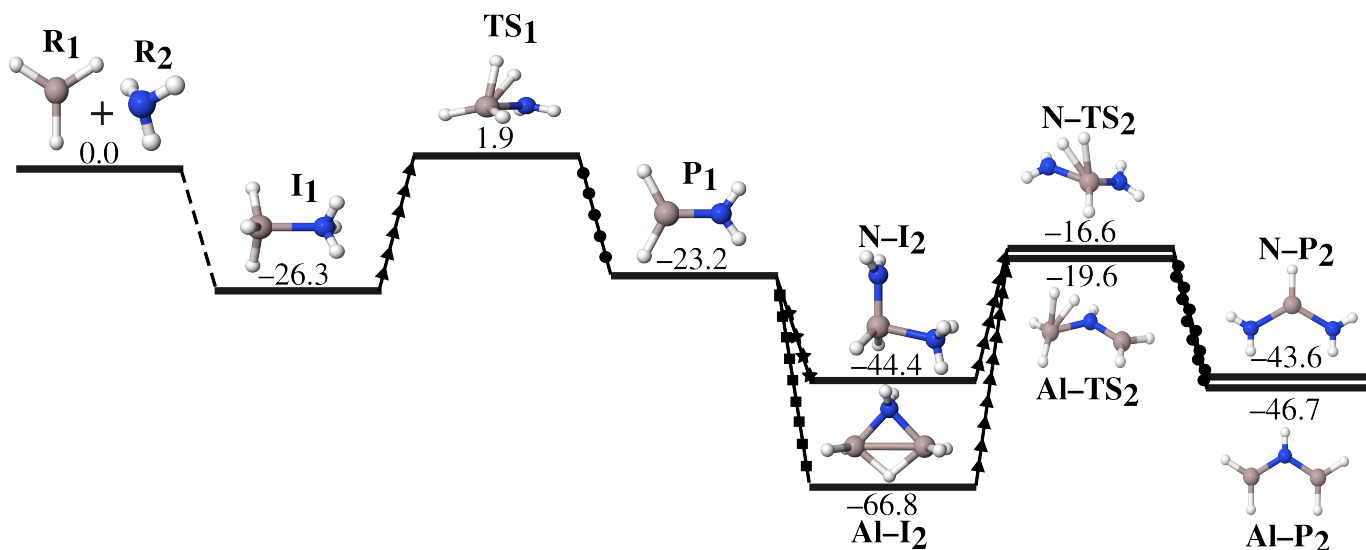


Figure 1. Reaction coordinate diagram from AlH_3 and NH_3 to N- and Al-P_2 . The arrowed lines indicate isomerization, the circular lines indicate H_2 departure, the starred lines indicate NH_3 addition, and the squared lines indicate AlH_3 addition. Relative energies are in kcal mol^{-1} . White atoms indicate H, blue atoms indicate nitrogen, and grey beige indicate Al.

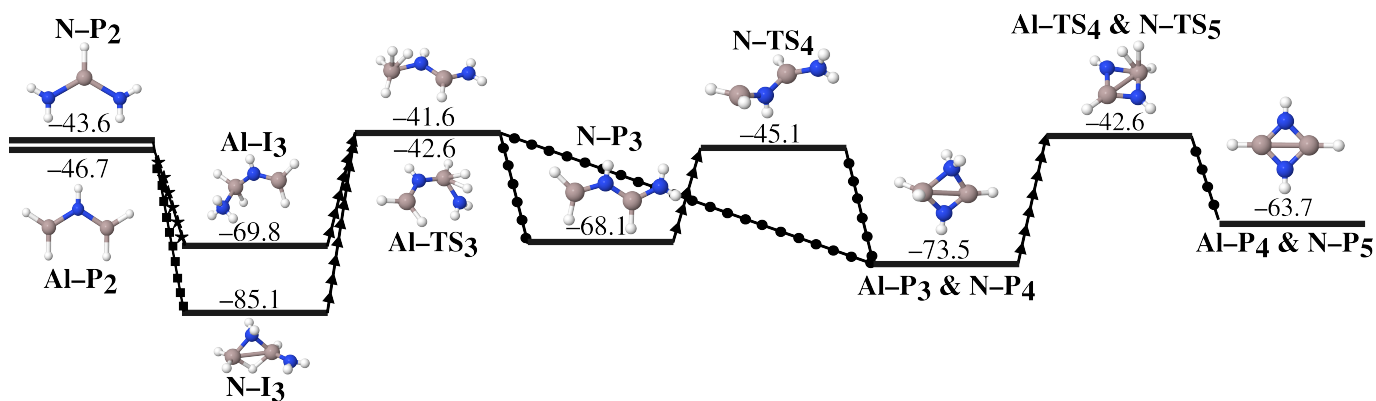


Figure 2. The continued reaction coordinate diagram from N- and Al-P_2 to cyclic- $\text{Al}_2\text{N}_2\text{H}_4$. The arrowed lines indicate isomerization, the circular lines indicate H_2 departure, the starred lines indicate NH_3 addition, and the squared lines indicate AlH_3 addition. Relative energies are in kcal mol^{-1} . White atoms indicate H, blue atoms indicate nitrogen, and grey beige indicate Al.

The molar absorption coefficients for each vibrational frequency are computed following the formula in EQ. 2 (Spanget-Larsen 2015), where " I_{IR} " is the IR intensity computed above and " w " is the resolving power of the given observing telescope.

$$\epsilon = 27.648 \times \frac{I_{IR}}{w} \quad (2)$$

The resolution, "R," of the NIRSpec and MIRI on the *JWST*, at their respective operating wavelengths, are provided and are trivially converted to the resolving power in EQ. 3 (Labiano, A. et al. 2021; Jakobsen, P. et al. 2022).

$$R = \frac{\lambda}{\Delta\lambda} \quad (3)$$

3. RESULTS AND DISCUSSION

3.1. Reaction Pathway Analysis

The reaction coordinate profile shown in Figs. 1 and 2 along with their corresponding equilibrium geometries, and definitions and chemical formulae in Table 1, shows the continual addition of equivalents of AlH_3 and NH_3 . Additions

Table 1. Symbol definitions and chemical formulae for the species in the present reaction pathway.

Symbol	Definition	Chemical Formula
R ₁	Reactant 1	AlH ₃
R ₂	Reactant 2	NH ₃
I ₁	Intermediate 1	AlNH ₆
TS ₁	Transition State 1	AlNH ₆
P ₁	Product 1	AlNH ₄
N-I ₂	Nitrogen Intermediate 2	AlN ₂ H ₇
Al-I ₂	Aluminum Intermediate 2	Al ₂ NH ₇
N-TS ₂	Nitrogen Transition State 2	AlN ₂ H ₇
Al-TS ₂	Aluminum Transition State 2	Al ₂ NH ₇
N-P ₂	Nitrogen Product 2	AlN ₂ H ₅
Al-P ₂	Aluminum Product 2	Al ₂ NH ₅
N-I ₃	Nitrogen Intermediate 3	Al ₂ N ₂ H ₈
Al-I ₃	Aluminum Intermediate 3	Al ₂ N ₂ H ₈
N-TS ₃	Nitrogen Transition State 3	Al ₂ N ₂ H ₈
Al-TS ₃	Aluminum Transition State 3	Al ₂ N ₂ H ₈
N-P ₃	Nitrogen Product 3	Al ₂ N ₂ H ₆
N-TS ₄	Nitrogen Transition State 4	Al ₂ N ₂ H ₆
Al-P ₃	Aluminum Product 3	Al ₂ N ₂ H ₆
N-P ₄	Nitrogen Product 4	Al ₂ N ₂ H ₆
Al-TS ₄	Aluminum Transition State 4	Al ₂ N ₂ H ₆
N-TS ₅	Nitrogen Transition State 5	Al ₂ N ₂ H ₆
Al-P ₄	Aluminum Product 4	Al ₂ N ₂ H ₄
N-P ₅	Nitrogen Product 5	Al ₂ N ₂ H ₄

of AlH₃ and NH₃ produce progressively larger datively-bonded structures but contain an initially raised transition barrier from I₁ to the P₁. In order for the reaction to progress to larger aluminum nitride systems, I₁ must overcome the aforementioned barriered TS₁ that sits 1.9 kcal mol⁻¹ higher than the reactants and lose an H₂ molecule to form P₁. This is in stark contrast with previous computed reaction schemes (Grosselin & Fortenberry 2022; Gobrecht et al. 2022) on AlH₃ and water that produce aluminum oxides with submerged barriers of formation. These barrierless formation most likely govern the short timescales of leading to the underdetection of a suitable carrier of the Al–O features, like Al₂O₃ in CSM or the ISM. Regardless, overcoming this barrier requires sufficiently high temperatures, ~960 K, in the aluminum nitride species’ formation environment from the surrounding stellar environments to begin forming larger clusters.

Obviously, the cold, diffuse ISM at ~10–40 K is not a likely region for the formation of P₁ to occur. However, as stated earlier, the previous work on Murchison CM2 (Zinner et al. 1991) suggests that the theorized aluminum nitride systems present in the meteorite may have nucleated the meteorite’s dust grain formation. If this is the case, then the aluminum nitride system would have been formed in some region warm enough for its own production and for dust grain formation to occur. The warm environments of inner protoplanetary disks can achieve a range of temperatures anywhere from 500–1500 K (Boss 1998) and contain ample material for molecular synthesis to begin that may potentially lead to seeding and nucleating processes of dust grain formation. Additionally, highly evolved asymptotic giant branch (AGB) stars are known to exhibit much higher temperatures within 1–2 stellar radii at 2000–3000 K compared to the warm inner protoplanetary disks (Maercker et al. 2022). AGB stars also contribute considerable dust forming material to their surrounding environment, and the ISM at large, given the stars substantial mass-loss rates (Höfner & Olofsson 2018; Ferrarotti & Gail 2006). If a region of CSM or the ISM contains sufficient temperatures and has the necessary material, the proper conditions toward formation the aluminum nitride species along the reaction pathway proposed herein will be satisfied. Once these aluminum nitrides have been formed, they may likely go on to contribute to dust grain nucleation and formation as suggested in the study of the Murchison CM2 meteorite.

Once the transitional barrier, shown in Fig. 1, is overcome there will be enough latent energy within the system to further progress through the now relatively submerged pathway of formation. Thus, the reaction pathway is no longer nearly as limited by the surrounding temperature and can further condense into larger and larger dust grains in both the warmer and cooler regions of the CSM or ISM. In any case, from the P_1 structure, additions of AlH_3 or NH_3 lead to either the $N-I_2$ or the $Al-I_2$ structure. The addition of the AlH_3 leads to a lower energy cyclic structure with a three-center two-electron bond commonly seen in trivalent species containing an empty p -orbital like aluminum and boron (Mayer 1989). Upon the loss of the H_2 molecule, seen in the $N/Al-TS_2$ species, both pathways lead to their respective products (P_2) of similar structure. Interestingly, if an equivalent of AlH_3 is added to $N-P_2$, it stabilizes into $N-I_3$, which is structurally similar to $Al-I_2$ with a three-center two-electron bond. The extra stability of the three-center two-electron bond in $N-I_3$ yields the lowest energy structure of the present reaction pathway. While $N-I_3$ is the lowest energy structure, the reaction pathway should still progress further not only due to the energy from the ambient temperature of its formation environments but also from collision with other molecular citizens present within the same regions.

Further departure of an H_2 molecule from $(N \text{ or } Al)-I_3$ yields the cyclic $Al-P_3$ structure, whereas $N-P_3$ is an open chain structure. The open-chain $N-P_3$ structure must overcome a torsional barrier before it becomes the cyclic $N-P_4$. At this point along the pathway, the paths of additions of AlH_3 and NH_3 converge to the same structure. After a final loss of an H_2 molecule in $Al-TS_4$ and $N-TS_5$, the proposed reaction pathway concludes with the final cyclic structure of $Al-P_4$ and $N-P_5$ ($Al_2N_2H_4$). This $Al_2N_2H_4$ species may then go on to form larger aluminum nitride clusters that potentially contribute to the nucleation and formation of dust grains in the universe. Given that the above reaction pathway contains no carbon- or oxygen-containing species, the present reaction pathway may contribute to the aluminum dust grain nucleation pathways in regions where the C/O ratio is ~ 1 . However, in oxygen-rich environments it may compete with the aluminum-oxygen pathways described in previous studies (Gail & Sedlmayr 1998, 1999; Gobrecht et al. 2022). This may not be the case for carbon-dominated environments, $C/O \geq 1$, given the lack of oxygen and the aluminum-carbon motif has yet to be characterized in CSM or the ISM in any form other than AlNC. Therefore, the reaction pathway investigated in this work may assist in the potential detection of aluminum-containing dust grain nucleation species that have gone undetected, and understudied, in the literature for decades.

Table 2. Rotational Constants for AlH_3 , $AlNH_4$, and $AlNH_6$

Const.	Units	AlH_3	$AlNH_4$	$AlNH_6$
A_e	MHz	133833.5	95478.0	49434.0
B_e	MHz	133833.5	13074.1	9048.5
C_e	MHz	66916.7	11499.5	9048.4
A_0	MHz	132407.6	95063.3	49154.6
B_0	MHz	132407.6	13015.9	8916.2
C_0	MHz	66034.4	11430.3	8916.4
A_1	MHz	131376.9	94810.8	49090.3
B_1	MHz	131376.9	12994.8	8913.7
C_1	MHz	65518.7	11412.4	8913.9
A_2	MHz	131652.0	94636.1	49025.6
B_2	MHz	131652.0	12999.7	8914.2
C_2	MHz	66346.6	11411.6	8914.4
A_3	MHz	131457.8	94432.1	48865.1
B_3	MHz	131457.8	13009.1	8920.6
C_3	MHz	65043.4	11418.4	8920.8
A_4	MHz	132824.6	94214.4	48926.0
B_4	MHz	132824.6	13012.7	8922.5
C_4	MHz	66244.7	11415.5	8922.7
A_5	MHz		95436.9	49035.0

Continued on next page

Table 2 – continued from previous page

Const.	Units	AlH ₃	AlNH ₄	AlNH ₆
B_5	MHz		13034.2	8927.4
C_5	MHz		11420.7	8927.6
A_6	MHz		95225.2	49144.2
B_6	MHz		12981.5	8881.5
C_6	MHz		11369.6	8881.7
A_7	MHz		95582.8	49064.1
B_7	MHz		13017.0	8918.3
C_7	MHz		11441.5	8918.5
A_8	MHz		97565.1	49309.6
B_8	MHz		13052.9	8904.7
C_8	MHz		11398.1	8904.9
A_9	MHz		93906.6	49191.6
B_9	MHz		12981.2	8878.7
C_9	MHz		11444.4	8878.9
A_{10}	MHz		94707.4	49146.8
B_{10}	MHz		12977.0	8807.8
C_{10}	MHz		11433.0	8808.0
A_{11}	MHz		93227.5	49487.3
B_{11}	MHz		12975.5	8900.9
C_{11}	MHz		11429.1	8901.0
A_{12}	MHz		96185.7	49145.0
B_{12}	MHz		13038.4	8875.0
C_{12}	MHz		11430.9	8875.3
μ	D	0.0	1.08	5.40

3.2. Rovibrational Spectroscopic Analysis

As stated previously, some of the aluminum nitride systems investigated in this work have little-to-no previous experimental or observational data of any type. Therefore, the computed rovibrational spectroscopic constants for R₁ (AlH₃), I₁ (AlNH₆), and P₁ (AlNH₄) as shown in Fig. 1 reported herein are reference data necessary for laboratory analysis and potential astrophysical detection. Presently, AlH₃ and AlNH₄ have Ar matrix spectroscopic data in the

Table 3. Quartic and sextic distortion constants in the Watson A-reduced Hamiltonian for AlNH₄ and AlNH₆

Const.	AlNH ₄	AlNH ₆
Δ_J	12.151 (kHz)	16.330 (kHz)
Δ_K	1.630 (MHz)	76.397 (kHz)
Δ_{JK}	192.297 (kHz)	55.756 (kHz)
δ_J	1.621 (kHz)	149.664 (mHz)
δ_K	140.576 (kHz)	-36.525 (kHz)
Φ_J	2.955 (mHz)	-33.349 (mHz)
Φ_K	122.517 (Hz)	-188.055 (Hz)
Φ_{JK}	2.261 (Hz)	-79.589 (Hz)
Φ_{KJ}	-9.071 (Hz)	268.269 (Hz)
ϕ_j	2.638 (mHz)	18.738 (μ Hz)
ϕ_{jk}	1.188 (Hz)	-9.396 (Hz)
ϕ_k	81.816 (Hz)	-57.226 (MH)

Table 4. Quartic and sextic distortion constants in the Watson S-reduced Hamiltonian for AlH₃, AlNH₄, and AlNH₆

Const.	AlH ₃	AlNH ₄	AlNH ₆
D_J	6.338 (MHz)	11.486 (kHz)	16.330 (kHz)
D_{JK}	-11.275 (MHz)	196.288 (kHz)	55.756 (kHz)
D_K	5.287 (MHz)	1.627 (MHz)	76.397 (kHz)
d_1	-31.927 (Hz)	-1.621 (kHz)	-149.664 (mHz)
d_2	158.915 (Hz)	-332.607 (Hz)	8.511 (mHz)
H_J	885.237 (Hz)	-3.890 (mHz)	-33.344 (mHz)
H_{JK}	-3.292 (kHz)	862.837 (mHz)	374.006 (mHz)
H_{KJ}	3.939 (kHz)	-4.307 (Hz)	1.725 (Hz)
H_K	-1.530 (kHz)	119.158 (Hz)	-1.474 (Hz)
h_1	-23.100 (mHz)	1.787 (mHz)	23.397 (μ Hz)
h_2	-34.752 (mHz)	3.422 (mHz)	-2.245 (μ Hz)
h_3	-52.810 (Hz)	851.524 (μ Hz)	-4.658 (μ Hz)

Table 5. Vibrational frequencies (cm⁻¹), IR Intensities (km mol⁻¹) with absorption cross sections in parentheses (10⁻¹⁴ cm²), and wavelength (μ m) for D_{3h} AlH₃

Mode	Symm.	Desc.	Harm.	Anharm.	f (σ)	λ	Expt. ^a
ν_1	A'_1	AlH Stretch	1951.4	1890.7	0 (0)	5.29	
ν_2	A_2''	OPB	710.5	707.8	387 (200)	14.13	697.8
ν_3	E'	Anti-sym. AlH Stretch	1955.7	1889.7	251 (40)	5.29	1882.8
ν_4	E'	HAlH Anti-sym. Bend	798.6	789.1	234 (100)	12.67	783.4
ZPT				4052.6			

^aExperimental Ar matrix FTIR spectroscopy (Chertihin & Andrews 1993).

literature, and AlNH₄ and AlNH₆ have had previous theoretical studies conducted. Several of the previous theoretical studies (Davy & Jaffrey 1995; Leboeuf et al. 1995; Marsh et al. 1992) for AlNH₄ and AlNH₆ only provide an analysis of the harmonic frequencies and their structural character. However, The work herein provides anharmonic vibrational frequencies and rotational spectroscopic constants at a more rigorous level of theory.

In order to provide a full rovibrational profile for the aluminum nitride species investigated herein, the equilibrium, vibrationally averaged, and vibrationally excited rotational constants are reported in Table 2. Also, the quartic and sextic distortion constants from the A- and S-reduced Watson Hamiltonians are given in Tables 3 and 4, respectively. Additionally, the formation pathways to larger aluminum nitride species assume the presence of AlH₃ in the same regions. As AlH₃ has not yet been observed in CSM or the ISM, perhaps a consequence of its rapid reaction with ammonia or water, the present study also provides the reference data for this species for completeness. To that end, the vibrational profile for AlH₃, AlNH₆, and AlNH₄ are given in Tables 5, 6, and 7, respectively.

As stated above, previous Ar matrix spectroscopic data (Chertihin & Andrews 1993) exists for AlH₃ and characterizes three of the four vibrational frequencies available, shown in Table 5. The out-of-plane bending mode, ν_2 , differs the furthest from experiment at 10 cm⁻¹ or 1.4%. The closest to experiment is ν_4 , the H–Al–H anti-symmetric bending motion, differing by 5.7 cm⁻¹ or 0.7%. While the F12-TZ anharmonic vibrational frequencies exhibit relatively large differences compared to experiment, it should be noted that Ar matrix spectroscopy is known to cause a shift in the true vibrational frequency (Pimentel & Charles 1963). Thus, most of the discrepancy between the current high-level quantum chemical computations and experiment should be attributed to the Ar matrix shifts. Further, previous computational studies of Al-containing species utilizing the F12-TZ methodology have produced vibrational frequencies within 0.4% of the gas-phase experimental value (Fortenberry et al. 2020). Given the higher-order, D_{3h} symmetry exhibited by AlH₃ the permanent dipole of this molecule is zero, thus rendering it undetectable *via* rotational spectroscopy. For this reason, the anharmonic vibrational frequencies computed in this work are even more crucial for potential spaced-based IR spectroscopic telescopes.

Further, AlH_3 exhibits very intense vibrational transitions with the ν_2 , out-of-plane bend being the most intense at 387 km mol^{-1} . Compared to the anti-symmetric stretch of H_2O at 70 km mol^{-1} and CO_2 at $\sim 475 \text{ km mol}^{-1}$, which are both considered to be intense transitions, the present ν_2 intensity should be considered intense enough for detection *via* IR spectroscopy even at low concentrations. Additionally, the other vibrational fundamentals of AlH_3 with intensities of 251 and 234 km mol^{-1} are also substantially greater than the aforementioned stretches in water and carbon dioxide. Looking at the spectral profile, ν_4 sits at $12.67 \mu\text{m}$ putting it around the $13 \mu\text{m}$ spectral feature that is typically used as an identifier for Al_2O_3 . While this does not really question Al_2O_3 's presence based on this spectral feature, it does posit the existence of another carrier of said spectral feature in CSM or the ISM that may be attributed to the present aluminum nitride system. Nevertheless, the computed vibrational data herein should be especially important for the detection of AlH_3 that would be supportive for confirming the reaction pathway of formation proposed in this work and from previous computational reaction pathways (Grosselin & Fortenberry 2022; Flint & Fortenberry 2023).

Table 6. Vibrational frequencies (cm^{-1}), IR intensities (km mol^{-1}) with absorption cross sections in parentheses (10^{-14} cm^2), and wavelength (μm) for C_{3v} AlNH_6

Mode	Symm.	Desc.	Harm.	Anharm.	f (σ)	λ
ν_1	E	NH Stretch	3588.9	3411.8	45 (5)	2.93
ν_2	A_1	Sym. NH Stretch	3468.8	3322.4	16 (2)	3.01
ν_3	A_1	Sym. AlH Stretch	1885.7	1819.2	36 (6)	5.50
ν_4	E	AlH Stretch	1865.1	1800.4	331 (50)	5.55
ν_5	E	NH2 Rocking	1665.3	1624.4	19 (3)	6.16
ν_6	A_1	HNAI Sym. Bend	1269.0	1207.8	135 (30)	8.28
ν_7	E	HAIN Rocking	790.8	779.1	271 (100)	12.84
ν_8	A_1	HAIN Sym. Bend	773.9	755.7	515 (200)	13.23
ν_9	E	OPB	706.8	666.1	15 (10)	15.01
ν_{10}	A_1	AlN Stretch	426.4	389.3	11 (20)	25.69
ν_{11}	E	OPB	372.6	352.2	2 (-)	28.40
ν_{12}	A_2	Torsion	119.4	21.4	1 (-)	467.29
ZPT				12724.7		

The first intermediate, AlNH_6 , exhibits the most notable vibrational transition intensities of the two formed structures studied herein, shown in Table 6. AlNH_6 's ν_8 frequency, the H–Al–N symmetric bending motion, at 515 km mol^{-1} is 30 km mol^{-1} larger than the CO_2 motion mentioned above. Further, AlNH_6 ν_4 , ν_6 , and ν_7 exhibit transition intensities of 331 , 135 , and 271 km mol^{-1} , respectively. While AlNH_6 exhibits multiple intense vibrational transitions, due to the nature of its synthesis, it may be a short-lived species as it will likely progress to AlNH_4 or regress back to the reactants. However, even with a relatively small concentration, its intense transitions may still be seen in the IR. Rotationally, AlNH_6 also exhibits the largest permanent dipole moment of the three molecules studied, at 5.40 D . Compared to the previously detected (Tenenbaum & Ziurys 2010) AlOH molecule with a permanent dipole of 1.11 D (Fortenberry et al. 2020), AlNH_6 may be a suitable candidate for potential radioastronomical observation, but may be limited by shorter lifetimes as discussed above. Regardless, like AlH_3 , AlNH_6 also exhibits spectral features in and around the $13 \mu\text{m}$ dust feature as well as the associated 11 , 20 and $28 \mu\text{m}$. Namely, the aforementioned ν_8 frequency, with the 515 km mol^{-1} intensity, sits directly at $13.23 \mu\text{m}$, as shown in Table 6. It should be noted that the mid-to far-IR regions where these features are located are dominated by larger dust grains than present potential grain nucleating species. Regardless, a laboratory and observational study of AlNH_6 is warranted utilizing the novel reference data provided herein in order to assist in the astrophysical detection of the first intermediate along an alternative pathway for formation for dust grains in CSM or the ISM.

The AlNH_4 molecule has both previous Ar matrix spectroscopic data (Himmel et al. 2000) and theoretical vibrational frequency computations (Watrous et al. 2021). The previous vibrational frequency studies are computed at the F12-TZ level of theory much like the rovibrational spectroscopic data provided herein. While the present computational study utilizes a normal coordinate system to compute the QFF procedure, the previous study utilizes a symmetry

Table 7. Vibrational frequencies (cm^{-1}), IR intensities (km mol^{-1}) with absorption cross sections in parentheses (10^{-14} cm^2), and wavelength (μm) for C_{2v} AlNH_4

Mode	Symm.	Desc.	Harm.	Anharm.	f (σ)	λ	Prev. ^{a/b}
ν_1	b_2	Anti-symm. NH stretch	3673.6	3495.9	27 (3)	2.86	–/3496.8
ν_2	a_1	Symm. NH Stretch	3582.7	3421.5	31 (4)	2.92	3499.7/3421.7
ν_3	b_2	Anti-symm. AlH stretch	1961.2	1895.3	257 (40)	5.28	1899.3/1895.5
ν_4	a_1	Symm. AlH Stretch	1957.5	1893.5	81 (10)	5.28	1891.0/1894.7
ν_5	a_1	Symm. HNAI stretch	1582.0	1552.1	28 (5)	6.44	1541.6/1552.7
ν_6	a_1	AlN stretch	836.9	822.5	217 (90)	12.16	818.7/822.7
ν_7	a_1	Symm HAIN stretch	757.2	747.1	51 (20)	13.39	755.0/747.9
ν_8	b_2	Anti-symm. HNAI stretch	732.6	717.5	145 (90)	13.94	769.8/715.9
ν_9	b_1	Al OPB	614.4	606.0	165 (100)	16.50	608.7/611.3
ν_{10}	a_2	Anti-symm. Torsion	495.0	469.5	0 (0)	21.30	–/465.8
ν_{11}	b_1	N OPB	448.9	442.9	236 (300)	22.58	518.3/426.1
ν_{12}	b_2	Anti-symm. HAIN stretch	426.0	422.8	19 (30)	23.65	–/431.4
ZPT				8427.6			

^a Previous Ar matrix attributions (Himmel et al. 2000).

^b Previous F12-TZ anharmonic vibrational data (Watrous et al. 2021).

internal coordinate system that is comparable to the present normal coordinate system. Any deviation between the two methods should be considered an effect of the difference between the construction of the two coordinate systems. In any case, while, AlNH_6 contains more intense vibration transitions, AlNH_4 still exhibits exceptionally intense transitions. Shown in Table 7, the AlNH_4 molecule’s most intense transition is its anti-symmetric Al–H stretching motion, ν_3 , of 257 km mol^{-1} . Like AlNH_6 , AlNH_4 also contains multiple intense vibrational transitions such as ν_6 , ν_8 , ν_9 , and ν_{11} at 217 , 145 , 165 , and 236 km mol^{-1} , respectively. Again, while most of these transitions are less intense than AlNH_6 , the above intensities are still relatively intense suggesting AlNH_4 is a strong candidate for potential astrophysical detection utilizing IR spectroscopy. Additionally, this species may be longer-lived in its formation environment in CSM making it an even stronger candidate for astronomical observational detection, perhaps, than AlNH_6 itself.

In terms of its dipole moment, the AlNH_4 molecule’s is much smaller at 1.08 D . While AlNH_4 can still be observed rotationally given a high enough column density, with such a small dipole moment AlNH_4 may be better suited for detection via high resolution IR spectroscopy which can be achieved *via* the JWST. Also, AlNH_4 contains multiple spectral features that fall in or around the $13 \mu\text{m}$ feature and other associated spectral lines. Specifically, ν_7 and ν_8 have wavelengths at 13.39 and $13.94 \mu\text{m}$, respectively, shown in Table 7. Again, this suggests that more than Al_2O_3 or the other associated suspected carriers exhibit this spectral feature, but this does suggest that species containing aluminum may contribute to the features more than initially observed or speculated. To that end, the novel vibrational spectroscopic data provided herein are necessary for further laboratory and possible astronomical observational investigations into the proposed formation pathway that will potentially assist in characterizing another potential player in dust grain formation.

4. CONCLUSIONS

The reaction pathway of AlH_3 and NH_3 leads to the formation of larger aluminum nitride molecular systems. This pathway must first overcome a barrier of $1.9 \text{ kcal mol}^{-1}$ which is fully achievable in high temperature environments ($\sim 1000 \text{ K}$) such as warmer inner protoplanetary disks and circumstellar envelopes of AGB stars, but not necessary to begin the process of formation. The rest of the pathway is submerged compared to the reactants and is available given the latent energy present in the molecular system. The final step of the presently studied pathway involves the formation of a four-membered cyclic ring that is also the only step on the pathway to have a submerged product over its preceding intermediate. Even so, the present reaction pathway provides a novel, potential formation mechanism for Al-bearing dust grains containing nitrogen as suggested in the studies of the Murchison CM2 chondritic meteorite and gives a hint at where such nucleation can take place in protoplanetary disks.

The AlNH_4 molecule investigated herein is the most likely candidate for potential astronomical observation *via* current rovibrational spectroscopic technologies in order to support this proposed reaction pathway. AlNH_4 contains

multiple vibrational transitions with exceptionally large intensities, notably the 1895.3 cm^{-1} frequency with the 257 km mol^{-1} intensity and the 442.9 cm^{-1} frequency with the 236 km mol^{-1} intensity. While AlNH_4 has a smaller dipole moment of 1.08 D , if there is sufficient column density, this species should still be observable utilizing current radioastronomical telescopes. The rovibrational analysis of AlNH_6 suggests that the most intense vibrational transition studied here is the 515 km mol^{-1} intensity corresponding to the 755.7 cm^{-1} frequency. Additionally, the 5.40 D dipole moment feature calculated is the largest of the three studied. However, given the AlNH_6 molecule's likely shorter timescales within the reaction pathway, it may not be a suitable candidate for rovibrational detection in CSM or the ISM. The AlH_3 molecule also exhibits exceptionally intense vibrational transitions, especially the 707.8 cm^{-1} frequency with an intensity of 387 km mol^{-1} . Like the AlNH_6 molecule, the AlH_3 molecule may react too quickly, with ammonia, water, or other circumstellar or interstellar denizens before it can be detected. However, the spectral features give it a strong chance of observation with *JWST*. That being said, while all three species contain strong IR features and some strong rotational features, AlNH_4 may be the most likely candidate for potential astronomical observation.

The three Al-containing molecules studied in the present work contain vibrational frequencies that fall in or around the $13\text{ }\mu\text{m}$ spectral feature attributed to Al–O class of molecules. Additionally, the computed vibrational profile shows the presence of vibrational frequencies at the associated 11 , 20 , and $28\text{ }\mu\text{m}$ carrier features. The spectral features found in the present Al-containing species imply that dust containing some form of aluminum oxide may not be the only source of the $13\text{ }\mu\text{m}$ dust feature, and the aluminum nitride species studied herein may provide other alternative answers to the question of the origins of such features. These computed vibrational analyses warrant further laboratory, theoretical, and observational investigations into the present reaction profile and other, higher-order aluminum nitride clusters. These investigations will assist in the search for Al-containing species that may be present in CSM and the ISM, but have been uncharacterized and understudied in the present literature.

5. ACKNOWLEDGMENT

This work is supported by NASA Grants NNH22ZHA004C and 22-A22ISFM-0009 and by the University of Mississippi's College of Liberal Arts. The computational support is from the Mississippi Center for Supercomputing Research funded in part by NSF Grant OIA-1757220. CZP would like to thank Dr. Brent R. Westbrook for his revision of this manuscript. The authors would like to thank the reviewer for their important insight in the introduction and discussion of this manuscript.

REFERENCES

- Adler, T. B., Knizia, G., & Werner, H.-J. 2007, *JChPh*, 127, 221106
- Agbaglo, D., & Fortenberry, R. C. 2019, *CPL*, 734, 136720
- Agbaglo, D., Lee, T. J., Thackston, R., & Fortenberry, R. C. 2019, *ApJ*, 871, 236
- Boss, A. P. 1998, *AREPS*, 26, 53
- Cernicharo, J., & Guélin, M. 1987, *A&A*, 183, L10
- Chang, C., Patzer, A. B. C., Sedlmayr, E., & Sülzle, D. 1998, *EPJD*, 2, 57
- Chertihin, G. V., & Andrews, L. 1993, *JPhCh*, 97, 10295
- Crawford, T. D., & Schaefer III, H. F. 2000, in *Reviews in Computational Chemistry*, ed. K. B. Lipkowitz & D. B. Boyd, Vol. 14 (New York: Wiley), 33–136
- Czyzak, S. J., Hirth, J. P., & Tabak, R. G. 1982, *VA*, 25, 337
- Danilovich, T., Van de Sande, M., Plane, J. M. C., et al. 2021, *A&A*, 655, A80
- Davy, R. D., & Jaffrey, K. L. 1995, *JPhCh*, 98, 8930
- Decin, L., Richards, A. M. S., Waters, L. B. F. M., et al. 2017, *A&A*, 608, A55
- Doerksen, E. S., & Fortenberry, R. C. 2020, *ESC*, 4, 812
- Dunning, T. H. 1989, *JChPh*, 90, 1007
- Ferrarotti, A. S., & Gail, H.-P. 2006, *A&A*, 447, 553
- Finney, B., Fortenberry, R. C., Francisco, J. S., & Peterson, K. A. 2016, *JChPh*, 145, 124311
- Flint, A., & Fortenberry, R. C. 2023, *ESC*, 7, 2119
- Fortenberry, R. C. 2017, *IJQC*, 117, 81
- Fortenberry, R. C., Huang, X., Crawford, T. D., & Lee, T. J. 2014, *JPCA*, 118, 7034
- Fortenberry, R. C., & Lee, T. J. 2019, *Ann. Rep. Comput. Chem.*, 15, 173
- Fortenberry, R. C., Lee, T. J., & Müller, H. S. P. 2015, *MolAs*, 1, 13
- Fortenberry, R. C., Novak, C. M., Layfield, J. P., Matito, E., & Lee, T. J. 2018, *J. Chem. Theor. Comput.*, 14, 2155
- Fortenberry, R. C., Trabelsi, T., & Francisco, J. S. 2020, *JPCA*, 124, 8834
- Franke, P. R., Stanton, J. F., & Doublerly, G. E. 2021, *JPCA*, 125, 1301

- Frisch, M. J., Trucks, G. W., Schlegel, H. B., et al. 2016, Gaussian 16 Revision C.01
- Gail, H.-P., & Sedlmayr, E. 1998, *FaDi*, 109, 303
- . 1999, *A&A*, 347, 594
- Gardner, M. B., Westbrook, B. R., Fortenberry, R. C., & Lee, T. J. 2021, *AcSpA*, 248, 119184
- Gobrecht, D., Cherchneff, I., Sarangi, A., Plane, J. M. C., & Bromley, S. T. 2016, *A&A*, 585, A6
- Gobrecht, D., Plane, J. M. C., Bromley, S. T., et al. 2022, *A&A*, 5658, A167
- Grosselin, D., & Fortenberry, R. C. 2022, *ESC*, 6, 18
- Himmel, H.-J., Downs, A. J., & Greene, T. M. 2000, *ChCom*, 871
- Höfner, S., & Olofsson, H. 2018, *A&ARv*, 26, 1
- Huang, X., Fortenberry, R. C., & Lee, T. J. 2013, *JChPh*, 139, 084313
- Huang, X., & Lee, T. J. 2008, *JChPh*, 129, 044312
- . 2009, *JChPh*, 131, 104301
- Huang, X., Taylor, P. R., & Lee, T. J. 2011, *JPCA*, 115, 5005
- Hutcheon, I. D., Huss, G. R., Fahey, A. J., & Wasserburg, G. J. 1994, *ApJ*, 425, L97
- Inostroza-Pino, N., Palmer, C. Z., Lee, T. J., & Fortenberry, R. C. 2020, *JMoSp*, 369, 111273
- Jakobsen, P., Ferruit, P., Alves de Oliveira, C., et al. 2022, *A&A*, 661, A80
- Kamiński, T. 2015, *Nature*, 520, 322
- Kamiński, T., Tylenda, R., Menten, K. M., et al. 2018, *NatAS*, 2, 778
- Kamiński, T., Wong, K. T., Schmidt, M. R., et al. 2016, *A&A*, 592, A42
- Kendall, R. A., Dunning, T. H., & Harrison, R. J. 1992, *JChPh*, 96, 6796
- Kitchens, M. J. R., & Fortenberry, R. C. 2016, *CP*, 472, 119
- Knizia, G., Adler, T. B., & Werner, H.-J. 2009, *JChPh*, 130, 054104
- Labiano, A., Argyriou, I., Álvarez-Márquez, J., et al. 2021, *A&A*, 656, A57
- Leboeuf, M., Russo, N., Salahub, D. R., & Toscano, M. 1995, *JChPh*, 103, 7408
- Lee, C., Yang, W. T., & Parr, R. G. 1988, *PhRvB*, 37, 785
- Lodders, K. 2003, *ApJ*, 591, 1220
- Maercker, M., Khouri, T., Mecina, M., & Beck, E. D. 2022, *A&A*, 663, A64
- Marsh, C. M. B., Hamilton, T. P., Xie, Y., & III, H. F. S. 1992, *JChPh*, 96, 5310
- Martin, J. M. L., & Kesharwani, M. K. 2014, *J. Chem. Theor. Comput.*, 10, 2085
- Martin, J. M. L., Lee, T. J., Taylor, P. R., & François, J.-P. 1995, *JChPh*, 103, 2589
- Martin, J. M. L., & Taylor, P. R. 1997, *AcSpA*, 53, 1039
- Mayer, I. 1989, *JMoSt*, 186, 43
- Mills, I. M. 1972, in *Molecular Spectroscopy - Modern Research*, ed. K. N. Rao & C. W. Mathews (New York: Academic Press), 115–140
- Møller, C., & Plesset, M. S. 1934, *PhRv*, 46, 618
- Nittler, L. R., Alexander, C. M. O., Gallino, R., et al. 2008, *ApJ*, 682, 1450
- Nuth, J. A. 1985, *Nature*, 318, 166
- Palmer, C. Z., & Fortenberry, R. C. 2022, *ESC*, 6, 2032
- Papousek, D., & Aliev, M. R. 1982, *Molecular Vibration-Rotation Spectra* (Amsterdam: Elsevier)
- Patzer, A. B. C., Chang, C., Sadlmayr, E., & Sülzle, D. 2005, *EPJD*, 32, 329
- Peterson, K. A., Adler, T. B., & Werner, H.-J. 2008, *JChPh*, 128, 084102
- Pimentel, G. C., & Charles, S. W. 1963, *PAPCh*, 7, 111
- Raghavachari, K., Trucks, G. W., Pople, J. A., & Head-Gordon, M. 1989, *CPL*, 157, 479
- Ramal-Olmedo, J. C., Menor-Salván, C. A., & Fortenberry, R. C. 2021, *A&A*, 656, A148
- Saberi, M., Khouri, T., Velilla-Prieto, L., et al. 2022, *A&A*, 663, A54
- Shavitt, I., & Bartlett, R. J. 2009, *Many-Body Methods in Chemistry and Physics: MBPT and Coupled-Cluster Theory* (Cambridge: Cambridge University Press)
- Sloan, G. C., Kraemer, K. E., Goebel, J. H., & Price, S. D. 2003, *ApJ*, 594, 483
- Spanget-Larsen, J. 2015, *Infrared Intensity and Lorentz Epsilon Curve from 'Gaussian' FREQ Output*
- Tenenbaum, E. D., & Ziurys, L. M. 2010, *ApJ*, L93
- Watrous, A. G., Davis, M. C., & Fortenberry, R. C. 2021, *FrASS*, 8, 1
- Watson, J. K. G. 1977, in *Vibrational Spectra and Structure*, ed. J. R. Durig (Amsterdam: Elsevier), 1–89
- Werner, H.-J., Knowles, P. J., Manby, F. R., et al. 2020, *WIREs Comput. Mol. Sci.*
- Westbrook, B. R., & Fortenberry, R. C. 2023, *J. Chem. Theory Comput.*, 19, 2606
- Westbrook, B. R., Patel, D. J., Dallas, J. D., et al. 2021, *JPCA*, 125, 8860
- Yang, W. T., Parr, R. G., & Lee, C. T. 1986, *PhRvA*, 34, 4586
- Yousaf, K. E., & Peterson, K. A. 2008, *JChPh*, 129, 184108
- Yu, Q., Bowman, J. M., Fortenberry, R. C., et al. 2015, *JPCA*, 119, 11623
- Zhao, D., Doney, K. D., & Linnartz, H. 2014, *ApJL*, 791, L28
- Zinner, E., Amari, S., Anders, E., & Lewis, R. 1991, *Nature*, 349, 51

Ziurys, L. M., Apponi, A. J., & Phillips, T. G. 1994, ApJ,
433, 729

Ziurys, L. M., Savage, C., Highberger, J. L., et al. 2002,
ApJ, 564, L45